HHS Public Access

Author manuscript

Dev Cell. Author manuscript; available in PMC 2017 May 09.

Published in final edited form as:

Dev Cell. 2016 May 9; 37(3): 267–278. doi:10.1016/j.devcel.2016.04.010.

Membrane supply and demand regulates F-actin in a cell surface reservoir

Lauren Figard[1,2], **Mengyu Wang**[1,3], **Liuliu Zheng**[1], **Ido Golding**[1,3,4,5], and **Anna Marie Sokac**[1,2]

[1]Verna & Marrs McLean Department of Biochemistry and Molecular Biology Baylor College of Medicine, Houston, TX 77030, USA

[2]Integrative Molecular and Biomedical Sciences Program Baylor College of Medicine, Houston, TX 77030, USA

[3]Graduate Program in Structural and Computational Biology and Molecular Biophysics Baylor College of Medicine, Houston, TX 77030, USA

[4]Center for the Physics of Living Cells University of Illinois at Urbana-Champaign, Urbana, IL 61801, USA

[5]Center for Theoretical Biological Physics Rice University, Houston, TX 77005, USA

Abstract

Cells store membrane in surface reservoirs of pits and protrusions. These membrane reservoirs facilitate cell shape change and buffer mechanical stress; but we do not know how reservoir dynamics are regulated. During cellularization, the first cytokinesis in *Drosophila* embryos, a reservoir of microvilli unfolds to fuel cleavage furrow ingression. We find that regulated exocytosis adds membrane to the reservoir before and during unfolding. Dynamic F-actin deforms exocytosed membrane into microvilli. Single microvilli extend and retract in ~20 seconds, while the overall reservoir is depleted *in sync* with furrow ingression over 60–70 minutes. Using pharmacological and genetic perturbations, we show that exocytosis promotes microvillar F-actin assembly, while furrow ingression controls microvillar F-actin disassembly. Thus, reservoir F-actin and, consequently, reservoir dynamics are regulated by membrane supply from exocytosis and membrane demand from furrow ingression.

Graphical abstract

Contact: Anna Marie Sokac, One Baylor Plaza, BCM125, Houston, TX 77030, USA, sokac@bcm.edu, Phone: (713) 798-3561, Fax: (713) 796-9438.

Author Contributions:

L.F., I.G., and A.M.S. designed experiments and interpreted data. L.F. conducted experiments and analyzed data. M.W. provided technical assistance with TIRF imaging and analyzed data. L.Z. generated Utrophin-mCherry flies. A.M.S. and L.F. wrote and edited the manuscript.

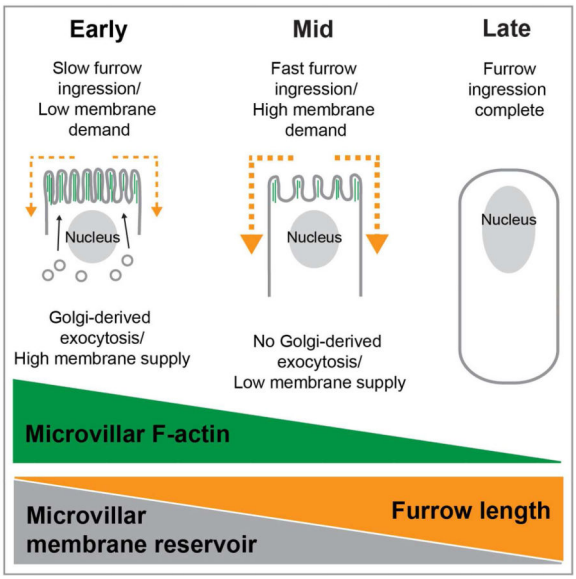

Introduction

Biologists have long recognized endocytosis and exocytosis as regulators of cell surface area. Yet, it is increasingly clear that membrane reservoirs, in the form of cell surface pits and protrusions, can also take up excess membrane to shrink cell surfaces, and release membrane to fuel cell surface growth (Clark et al., 2014; Figard and Sokac, 2014). For example, as apparent cell surface area gets smaller during apical cell constriction in gastrulating embryos, or during oscillatory contractions in cultured cells, membrane reservoirs of blebs, folds, and filopodia form (Kapustina et al., 2013; Martin et al., 2010; Nowotarski et al., 2014; Sweeton et al., 1991). Conversely, to prevent plasma membrane rupture during mechanical stretching in human myotubes and endothelial cells, reservoirs of surface invaginations flatten out (Cheng et al., 2015; Sinha et al., 2011). Membrane is transferred to and from reservoirs as cells change their shape in cytokinesis, cell spreading, phagocytosis, and tissue morphogenesis (Figard et al., 2013; Gauthier et al., 2011; Masters et al., 2013; Sedzinski et al., 2011; Tan and Zaidel-Bar, 2015). Thus, the sheer number and diversity of biological processes in which reservoirs participate argue that they represent a fundamental mechanism used by cells to control surface area.

Despite the prevalence of reservoirs, we have limited knowledge of how they are regulated, and how their usage is coordinated with endo- and exocytosis during cell shape change (Clark et al., 2014; Figard and Sokac, 2014). At the morphological level, most reservoirs are not membrane alone, but also contain protein scaffolds. The regulation of reservoirs is then likely to depend on regulation of their underlying scaffolds. For example, caveolae constitute a small membrane reservoir, storing <1% of cell surface area in invaginations supported by caveolar protein complexes (Sinha et al., 2011). Inactivation of caveolar complex formation blocks reservoir formation, and disassembly of the caveolar complexes upon cell stretching correlates with reservoir depletion (Cheng et al., 2015; Sinha et al., 2011). Thus, mechanical and/or molecular signals acting on the caveolar scaffold control reservoir formation and

utilization. For larger membrane reservoirs, such as microvilli or folds, which store >10% of cell surface area, the scaffold is F-actin (Figard and Sokac, 2013; Herant et al., 2005). However, F-actin scaffolds in these larger reservoirs are yet to be characterized at any level. We do not know if reservoir F-actin is highly dynamic, as in the cell surface protrusions of motile cells (Pollard and Borisy, 2003), or more stable, as in stereocilia or brush border microvilli (Rzadzinska, 2004; Tyska and Mooseker, 2002). Therefore, no clear predictions have been made regarding the regulation of F-actin scaffolds in reservoirs, even in the simplest cell types.

In addition to scaffolds, reservoir regulation is likely coupled to membrane trafficking, since endo- and exocytosis control the actual amount of membrane at cell surfaces (Gauthier et al., 2012; 2009). Endo- and exocytosis make significant and indisputable contributions to cell surface homeostasis and cell shape change, with demonstrated roles in many of the same events as reservoirs (Gauthier et al., 2011; Groulx et al., 2007; Lecuit and Wieschaus, 2000; Masters et al., 2013). But it remains unclear how membrane trafficking and reservoirs work together to manage membrane supply and demand at cell surfaces. In the case of cultured cells, reservoirs can complement membrane trafficking because membrane amounts can be managed by reservoirs on faster timescales than endo- and exocytosis (Charras et al., 2005; Erickson and Trinkaus, 1976; Kapustina et al., 2013; Sedzinski et al., 2011). For example, surface area expansion is biphasic during phagocytosis and cell spreading in cultured cells, with membrane for an initial fast phase of growth coming from reservoir unfolding, and membrane for a second slow phase provided by exocytosis (Gauthier et al., 2011; Masters et al., 2013). Thus, in cultured cells, reservoir unfolding and exocytosis work sequentially; with the signal to switch to exocytosis provided by a sudden increase in plasma membrane tension once the reservoir runs out (Gauthier et al., 2011; Masters et al., 2013). Whether this sequential use of external then internal membrane stores is universal versus context-dependent remains an open question. Other possibilities such as a reversed order of, or even simultaneous use of, exocytosis and reservoir unfolding have yet to be tested.

Drosophila cellularization offers a dramatic example of cell surface growth, during which the role for reservoir unfolding is now well established (Figard et al., 2013; Figard and Sokac, 2014; Fullilove and Jacobson, 1971; Lecuit and Wieschaus, 2000). Cellularization is the first tissue-building event in *Drosophila* development. In these embryos, the first 13 mitotic cycles occur with no intervening cytokinesis, generating a syncytium. Then, during cellularization at cell cycle 14, membrane furrows form at the embryo surface and simultaneously ingress between ~6000 nuclei to build a sheet of epithelial cells that are 35 μm tall (Figure 1A). Cellularization increases the embryo's surface area ~25-fold (Lecuit and Wieschaus, 2000). Exocytosis contributes some membrane for cellularization (Burgess et al., 1997; Lecuit and Wieschaus, 2000; Lee and Harris, 2014; Murthy et al., 2010; Sisson et al., 2000). However, apical microvilli also serve as a membrane reservoir, supplying approximately half of the membrane required for furrow ingression (Figard et al., 2013). Membrane depletion from the reservoir is controlled by furrow ingression itself, and microvillar membrane slides along the cell surface into growing furrows (Figard et al., 2013). Although both exocytosis and reservoirs have been implicated in cellularization, how their usage is regulated and coordinated is still mysterious. What's more, how reservoir

behavior during cellularization either relates to or is influenced by the underlying F-actin scaffold is not known.

Here, we track membrane and F-actin in the microvillar reservoir during cellularization. We show that exocytosis adds to the microvillar reservoir prior to and as the reservoir is depleted, unlike the sequential use of reservoirs followed by exocytosis, as predicted from cell culture work. Dynamic F-actin continually pushes excess reservoir membrane up into dynamic microvilli to create a transient and highly plastic storage compartment; and depletion of reservoir F-actin occurs *in sync* with depletion of reservoir membrane. Finally, we find that microvillar F-actin assembly and persistence of the reservoir depends on exocytosis, while F-actin disassembly and depletion of the reservoir is controlled by furrow ingression.

Results

Exocytosis delivers membrane that is stored in a microvillar reservoir

We recently showed that an apical reservoir of microvilli unfolds to provide membrane for furrow ingression during cellularization (Figard et al., 2013). Earlier studies showed that exocytosis also plays a role in furrow ingression during cellularization; and this exocytosis occurs apically, where the microvilli are (Burgess et al., 1997; Figard et al., 2013; Lecuit and Wieschaus, 2000; Mavor et al., 2016; Murthy et al., 2010; Sisson et al., 2000). To then reconcile how reservoir unfolding and exocytosis both contribute to cellularization, we examined the possibility that apically-directed exocytosis supplies membrane that is stored in microvilli until transfer to ingressing furrows. In earlier studies, the drug Brefeldin A (BFA) was used to block Golgi-derived, apically-directed exocytosis in cellularizing embryos (Frescas et al., 2006; Sisson et al., 2000). BFA shuts down secretory trafficking from the ER to Golgi, resulting in collapse of the Golgi and blockage of secretion (Frescas et al., 2006; Sciaky et al., 1997). To confirm this BFA activity in our experiments, we first examined the drug's effect in embryos expressing the Golgi marker, GFP-tagged Galactosyltransferase (GalT-GFP) (Snapp et al., 2004). In DMSO-injected control embryos, GalT-GFP labeled punctate Golgi bodies, which represent the normal Golgi structure in *Drosophila* embryos (Frescas et al., 2006; Snapp et al., 2004). In BFA-injected embryos, we saw significant collapse of the Golgi bodies within ~6 minutes of injection (Figure S1A), supporting BFA's ability to block exocytosis of Golgi-derived vesicles in cellularizing embryos.

To then ask whether apical exocytosis supplies membrane to the microvillar reservoir, we injected BFA immediately after the onset of cellularization (Figure 1A; 14Early (14E)), and assayed for the premature depletion of microvilli as furrows ingressed. Microvilli were tracked by collecting Z-stacks over time (4D imaging) at the apical surface of embryos expressing plasma membrane probe PLCδ Pleckstrin Homology Domain (Venus-PH-PLCδ; Figure 1B, 1C; Figard et al., 2013). For each time frame, Z-stacks were collapsed into maximum intensity Z-projections, and fluorescence intensity quantified (Figure 1B, 1D; Figure S1B; Figard et al., 2013). We found that microvillar membrane is depleted significantly faster in BFA-injected embryos than in controls, suggesting that blocking exocytosis reduces the microvillar reservoir (Figure 1C, 1D; Figure S1B). After 45 minutes,

the surface of BFA embryos looked smoother than the surface of control embryos. In fact, the surface of BFA embryos after 45 minutes appeared more similar to the surface of control embryos at the very end of cellularization, when almost all microvilli are gone and only lateral cell edges are apparent (Figure 1C; Figard et al., 2013). Thus, when exocytosis is blocked at 14E, membrane from the reservoir is prematurely exhausted. We believe that this result reflects a shortage of membrane supply, not an increase in membrane demand, since the rate of furrow ingression is the same in control and BFA-injected embryos (compare slow phase ingression rates for DMSO controls at 0.20 ± 0.02 μm/minute and BFA-injected embryos at 0.18 ± 0.01 μm/minute; N>6 embryos per condition; mean ± SE). Thus, our data support the idea that, during early cellularization, exocytosis of Golgi-derived vesicles adds membrane to the apical cell surface where it is temporarily caught up and stored in microvilli.

Since the microvilli provide membrane for furrow ingression (Figard et al., 2013), we predicted that BFA-injected embryos, with their reduced microvillar reservoir, would also have reduced final furrow lengths. To test this, we again injected BFA at cellularization onset (14E). However, this time we injected embryos expressing GFP-tagged Myosin-2 Regulatory Light Chain/Spaghetti Squash (Sqh-GFP; Royou et al., 2004). Sqh-GFP labels the furrow tips, allowing us to track furrow length versus time by confocal imaging at the embryo cross-section. We then measured final furrow lengths <80 minutes after cellularization onset. As predicted, we found that BFA injection at 14E resulted in shorter final furrow lengths compared to DMSO-injected controls (Figure 1E). Thus, microvilli are depleted faster and furrow length is shorter when exocytosis is blocked from the beginning of cellularization. Our data are consistent with a trajectory whereby membrane moves via exocytosis to an apical microvillar reservoir, and then to ingressing furrows.

To better map when exocytosis occurs and to determine how much membrane is added to the apical cell surface, we next performed timed BFA injections. We measured membrane “amount” in terms of final furrow lengths. These lengths clearly differed depending on when BFA was injected: BFA injection at the 13th cell cycle (13; Figure 1A) resulted in very short final furrow lengths (Figure 1E). In contrast, BFA injection at mid-cellularization, at the transition from the slow to fast phases of ingression and microvillar depletion (14M; Figure 1A; Figard et al., 2013), had no effect, with furrows ingressing to normal lengths (Figure 1E). Since furrows ingress normally after BFA injection at 14M, it is unlikely that off-target drug effects account for furrow inhibition after the earlier timed BFA injections (compare fast phase ingression rate for DMSO controls at 0.92 ± 0.05 μm/minute and BFA embryos at 0.95 ± 0.03 μm/minute; N=8 embryos per condition; mean ± SE). Rather, the timed BFA injections at 13, 14E, and 14M suggest the following sequence of events for the exocytosis of Golgi-derived membrane during cellularization: Prior to cellularization, a modest reservoir of membrane already exists at the cell surface. Then during the cycle 13–14E transition, a burst of exocytosis adds even more membrane to the reservoir, such that ~60% of the membrane required for furrow ingression is available (roughly 20 μm of a total 33 μm furrow length). This estimate agrees with previous scanning electron microscopy (SEM) analysis, showing that apical microvilli contain membrane sufficient for ~42–65% of furrow length at the onset of cellularization (Figard et al., 2013). Finally, within the first half of

cellularization, the remaining membrane required for furrow ingression is exocytosed to the apical microvillar reservoir (Figure 1E).

As a final confirmation that exocytosis builds the microvillar reservoir, we tracked apical membrane levels using Casein Kinase-1/Spider-GFP, a membrane probe for secretory vesicles that was previously used to detect newly exocytosed plasma membrane (Babu, 2002; Frescas et al., 2006). We predicted that levels of new apical membrane would increase between cycles 13 and 14E, as reservoir membrane would be augmented by exocytosis, but not yet depleted by furrow ingression. As expected, we found that Spider-GFP signal increases in microvilli between cycles 13 and 14E in control embryos (Figure S1C, S1D). To confirm that this membrane increase is due to exocytosis, we injected BFA in cycle 13, and saw that the Spider-GFP increase at the cycle 13 to 14E transition was significantly reduced (Figure S1C, S1D). We conclude that the microvillar membrane reservoir is fed by apically directed exocytosis largely prior to, but also coincident with, the reservoir unfolding that fuels cleavage furrow ingression. This is in contrast to prior observations for cell spreading and phagocytosis in cultured cells where reservoirs unfold first, and then exocytosis provides new membrane afterward (Gauthier et al., 2011; Masters et al., 2013).

Dynamic F-actin supports a dynamic microvillar membrane reservoir

Given that the microvillar membrane reservoir is large, containing enough membrane for ≥20 μm of furrow growth, it likely requires a scaffold to support its structure and prevent unwanted fission, fusion, and “pearling” events (Heinrich et al., 2014). Consistent with that, we confirmed that F-actin underlies the microvillar reservoir in cellularizing embryos (Figure 2A, 2B; Grevengoed, 2003).

Unlike F-actin in brush border microvilli, which is relatively stable (Crawley et al., 2014), we predicted that F-actin in the embryonic microvilli would be highly dynamic because: 1) the microvilli, as seen by SEM, resemble dynamic F-actin protrusions, such as filopodia and ruffles (Figard et al., 2013); and 2) previous live imaging showed that the apical cell surface is covered with dynamic “villous” membrane protrusions (Fabrowski et al., 2013). Thus, to follow F-actin dynamics, we used total internal reflection fluorescence (TIRF) microscopy to image F-actin at the surface of cellularizing embryos. Embryos expressing fluorescent F-actin marker, Utrophin-mCherry (Burkel et al., 2007), were imaged at one-second intervals during early cellularization. We observed foci that increased and decreased in fluorescence with the duration of 16.6 ± 6.6 seconds (N=76 MV, mean ± SD; Figure 2C, 2D, 2G; Movie S1). We interpreted these foci to be individual microvilli, extending and retracting into and out of the imaging plane in a “head-on” orientation (Figure 2B). To confirm that foci are protrusions and not invaginations, we looked at cell edges where fluorescence signal is sparser and microvilli tend to lay down parallel to the imaging plane (Figure 2B; Figard et al., 2013). Here, F-actin fingers were seen extending and retracting with the duration of 19.6 ± 8.9 seconds (N=62 MV, mean ± SD; Figure 2E, 2F, 2G; Movie S1), similar to the lifespan of the foci observed in the “head-on” orientation. As a negative control, we confirmed that gastrulating embryos, which lack microvilli on their surface (Martin et al., 2010; Sweeton et al., 1991), do not show these Utrophin-mCherry features (Figure 2H). These results suggest that the microvilli are dynamic membrane protrusions, supported by dynamic F-actin.

We tested if F-actin dynamics in microvilli are driven by actin polymerization and depolymerization. First, we used fluorescence recovery after photobleaching (FRAP) to quantify microvillar F-actin dynamics. We used rhodamine G-actin as our probe because, when incorporated into filaments, it was brighter than Utrophin-mCherry, and so allowed us to bleach and image F-actin recovery at the embryo cross-section. Wild-type embryos were injected with rhodamine G-actin ~15 minutes before cellularization to allow diffusion throughout the large embryo (Cao et al., 2008). Microvillar F-actin was photobleached in a $3\mu m^2$ box at the apical cell surface (Figure 3A, 3B). Bleached F-actin signal turned over rapidly with a half time to recovery of 14.4 ± 2.1 seconds and mobile fraction of 98 ± 4% (N=24 embryos, mean ± SE). To be certain that recovery was a result of F-actin turnover, rather than G-actin diffusion, we also injected embryos with F-actin stabilizer, Phalloidin, before bleaching. Phalloidin blocked FRAP (Figure 3A, 3B), indicating that recovery occurs by F-actin polymerization and depolymerization.

Next, we asked if F-actin polymerization is required to maintain microvilli. We imaged microvilli in embryos expressing F-actin probe Utrophin-mCherry, immediately after injection with Latrunculin A (LatA; Figure 3C-3E). LatA is a drug that binds G-actin and prevents its incorporation into filaments (Coué et al., 1987). Because LatA did not have time to diffuse throughout the embryo, it showed a graded effect with increasing distance from the injection site: Near the injection site, microvillar F-actin signal was strongly reduced. Further from the injection site (~100 μm away), microvillar F-actin signal remained at control levels (Figure 3D, 3E). Specifically, F-actin fluorescence intensity near the injection site decreased to 51.2 ± 3.6% of the control level (N=5 embryos; mean ± SE). Thus, microvillar F-actin appears to rapidly disassemble when F-actin polymerization is blocked by LatA injection. So far, our results support a model whereby exocytosis delivers excess membrane to the apical cell surface, where dynamic F-actin pushes the membrane up into microvilli for storage until transfer to ingressing furrows.

Microvillar F-actin is depleted in sync with microvillar membrane and furrow ingression

To then release membrane from the microvillar reservoir, we hypothesized that the underlying F-actin scaffold must be disassembled. But how is microvillar F-actin disassembly related to the liberation of microvillar membrane and furrow growth? To address this question we tracked the kinetics of microvillar F-actin depletion in Utrophin-mCherry embryos, using 4D imaging. We found that microvillar F-actin is depleted in an early slow phase followed by a later fast phase (Figure 4A, 4B). Furrow ingression and microvillar membrane depletion also occur in an early slow phase and a later fast phase (Figure 1A, S2A–S2C; Figard et al., 2013; Lecuit and Wieschaus, 2000; Papoulas et al., 2004; Royou et al., 2004). Thus, we asked whether the biphasic depletion of microvillar F-actin and membrane occur *in sync* with each other. By relating 4D depletion data for microvillar F-actin (Figure 4B) to 4D depletion data for microvillar membrane (Venus-PH-PLCδ; Figure S2A), we saw that F-actin and membrane depletion are linearly coupled throughout cellularization (Figure 4C). The same linear coupling was observed between microvillar F-actin and the additional membrane probe, Spider-GFP (Figure S2C, S2D). This coupling supports the idea that F-actin disassembly allows for the release of membrane from microvilli.

To next ask how microvillar F-actin depletion and furrow growth are related, we compared 4D microvillar F-actin depletion (Figure 4B) to furrow ingression data (Sqh-GFP; Figure S2B). We found that microvillar F-actin is depleted linearly with increasing furrow length (Figure 4D). These results suggest that microvillar F-actin depletion, microvillar membrane depletion, and far away furrow growth are all kinetically coupled with each other. Since our earlier SEM analysis showed that microvillar density, not size, decreases linearly with increasing furrow length (Figard et al., 2013), we suggest that membrane for furrow growth is liberated by antagonizing the growth of or promoting the disassembly of more and more microvillar F-actin cores.

Microvillar F-actin disassembly is coupled to furrow ingression

Because microvillar F-actin depletion is kinetically coupled to furrow ingression (Figure 4D), and the microvilli provide the membrane for furrow ingression (Figard et al., 2013), we hypothesized that the demand for membrane during furrow growth controls the disassembly of microvillar F-actin. If correct, then impaired furrow growth should correlate with increased microvillar F-actin levels. Thus, we developed a method to locally block furrow ingression within an embryo and then correlate furrow blockage with local microvillar F-actin levels: We injected Utrophin-mCherry embryos with a high dose of fluorophore-conjugated lectin (0.5 mg ml^{-1} Alexa488-Wheat Germ Agglutinin; WGA^{Ax488}) at the onset of cellularization. WGA binds glycosylated proteins on nuclear membranes (Davis and Blobel, 1986; Holt et al., 1987); and when injected at high concentration, the heterodimeric WGA caused adjacent nuclear membranes to stick together. Because ingressing furrows normally pass between the nuclei, WGA^{Ax488} crosslinked nuclei formed an obstacle to ingression (Figure 5A-5D; note that channels are pseudocolored for presentation). This obstacle was localized immediate to the injection site, because the WGA^{Ax488} concentration was highest there (Figure 5B, 5D). Further from the injection site, furrow ingression was not disrupted. Since all furrow tips are integrated in a hexagonal network, a bowed furrow front resulted, with short furrows at the injection site and long furrows further off (Figure 5B, 5D, 5F, 5H; Figure S3B). To confirm that bowing was not caused by injection alone, we assayed furrow lengths and microvillar F-actin intensities in buffer-injected control embryos, and found them to be the same regardless of distance from the injection site (Figure 5C, 5E, 5G; Figure S3A).

For embryos with WGA^{Ax488} crosslinked nuclei, we related the continuum of different furrow lengths to the coincident apical F-actin levels at ~40 minutes post injection. Per embryo, we observed three distinct “zones” (Figure 5D, 5F, and 5H; Figure S3B). In the zone furthest from the injection site (Zone 3), furrows were longest, and microvillar F-actin fluorescence was at an intermediate level (Figure 5D, 5F, 5H; Figure S3B). The appearance of furrows and microvillar F-actin depletion in Zone 3 resembled that in buffer-injected control embryos at the same post-injection time (Figure 5C). Thus, Zone 3 represents an internal control for normal ingression and microvillar F-actin depletion. In a transition Zone 2 (indicated by gray shading in Figure 5F, 5H; Figure S3B), spanning between Zone 3 and the WGA^{Ax488} crosslinked nuclei, furrow lengths were progressively shorter, and the corresponding microvillar F-actin levels were higher than in Zone 3 (Figure 5D, 5F, 5H; Figure S3B). Thus, where furrow ingression is impeded, there is a reciprocal increase in

microvillar F-actin. This result supports our hypothesis that furrow ingression regulates and promotes microvillar F-actin disassembly.

Microvillar F-actin assembly is promoted by exocytosis

Counter to our expectations, however, in Zone 1, the region closest to the injection site, the furrows were shortest, and the apical F-actin levels were lowest (Figure 5D, 5F, 5H; Figure S3B). We reasoned that if WGA^{Ax488} crosslinking between nuclei blocks basally directed furrow ingression, perhaps crosslinking also blocks apically directed transport of membrane vesicles and secretion. If the apically directed vesicles contain either membrane or F-actin regulators that promote microvillar F-actin assembly, then a blockage of trafficking and exocytosis could explain the surprising deficit of microvillar F-actin in Zone 1.

To first test whether nuclear crosslinking can block membrane traffic to the apical surface, we injected Alexa594-conjugated WGA (WGA^{Ax594}) into GalT-GFP embryos (Frescas et al., 2006; Snapp et al., 2004). Previously, GalT-GFP labeled Golgi bodies were observed to traffic along the apical-basal axis of forming cells during cellularization (Frescas et al., 2006). As above, we imaged the embryos ~40 minutes after WGA^{Ax594} injection. In buffer-injected control embryos, GalT-GFP fluorescence below all nuclei remained constant regardless of position from the injection site (Figure 6A, 6C; Figure S4A; note that the GalT-GFP channel is pseudocolored for presentation). In contrast, in WGA^{Ax594}-injected embryos, GalT-GFP signal below the crosslinked nuclei was elevated compared to regions far from the injection site (Figure 6B, 6D; Figure S4B). We saw a similar accumulation of Spider-GFP labeled secretory vesicles under WGA crosslinked nuclei, supporting that crosslinked nuclei prevent apically directed membrane trafficking and exocytosis (Figure S5A, S5B). To then test whether blocked exocytosis could account for the depletion of microvillar F-actin in Zone 1, we returned to our timed BFA injection strategy. We injected BFA in embryos at 14E (Figure 1A), and fixed and stained with Alexa488-Phalloidin ($Phalloidin^{Ax488}$). Whereas $Phalloidin^{Ax488}$ labeled F-actin in furrow tips in both DMSO-injected control and BFA-injected embryos, $Phalloidin^{Ax488}$ did not label the apical surface of BFA-injected embryos (Figure S5C). This result suggests a specific and dramatic inhibition of microvillar F-actin assembly in BFA embryos. To further establish a causal relationship between exocytosis and microvillar F-actin, we performed 4D imaging of live Utrophin-mCherry embryos injected with BFA at 14E. Similar to the impact of BFA injection on microvillar membrane (Figure 1C, 1D; Figure S1B), microvillar F-actin was depleted significantly faster when apically-directed exocytosis was blocked (Figure 6E, 6F; Figure S5D). Thus, membrane addition by exocytosis makes a permissive environment for F-actin assembly. These results suggest that apical exocytosis not only supplies the membrane that is stored in the microvillar reservoir, but it also promotes assembly of the dynamic F-actin scaffold under that reservoir. When apical exocytosis is reduced by experimental perturbation, or naturally as in the fast phase of cellularization, microvillar F-actin trends towards disassembly.

Microvillar F-actin disassembly is controlled by furrow ingression

Microvillar F-actin is depleted *in sync* with furrow ingression, and the extent of microvillar F-actin disassembly correlates with furrow length. Thus, we asked if microvillar F-actin

disassembly is controlled by furrow ingression. We tracked microvillar F-actin depletion in Utrophin-mCherry embryos following RNAi knockdown of the furrow component Slam (*slam*^{RNAi}). Slam protein localizes to furrow tips, and genetic or RNAi knockdown of Slam induces well-characterized furrow ingression defects by preventing the normal recruitment of RhoGEF2, Rho1-GTPase, and Myosin-2 to furrow tips (Acharya et al., 2014; Figard et al., 2013; Lecuit et al., 2002; Stein et al., 2002; Wenzl et al., 2010). We immediately saw that more microvillar F-actin persisted at the end of cellularization in *slam*^{RNAi} embryos compared to buffer-injected controls (Figure 7A; Utrophin-mCherry depleted by 18.0 ± 1.7% at the end of cellularization in *slam*^{RNAi} versus 58.7 ± 2.2% in controls; N=12 and 6 embryos, respectively; mean ± SE). Using *slam*^{RNAi} in Sqh-GFP embryos, we confirmed that *slam* knockdown led to furrows that ingressed slower and to a lesser extent than buffer controls (Figure 7B). Coincident with these furrow ingression defects, we used 4D imaging to show that microvillar F-actin was also disassembled slower and to a lesser extent after *slam*^{RNAi} (Figure 7C). Thus, the correlation observed between F-actin disassembly and furrow length in the WGA^{AX488} crosslinking experiments is confirmed by *slam*^{RNAi}. In addition, the *slam*^{RNAi} data supports a model whereby furrow ingression regulates microvillar F-actin disassembly and consequent reservoir unfolding.

Discussion

Here we show that reservoir F-actin and, consequently, reservoir dynamics are regulated by membrane supply from exocytosis and membrane demand from furrow ingression. We find that F-actin in the microvillar reservoir of cellularizing embryos is significantly different than F-actin in other types of non-reservoir cell surface protrusions. These differences may reflect the unique requirements of an F-actin scaffold that is plastic enough to either store or release membrane on demand. For example, reservoir microvilli are comparable in length and diameter to gut microvilli and filopodia (Breitsprecher et al., 2011; Figard et al., 2013; Medalia et al., 2007; Mooseker and Tilney, 1975). Yet, F-actin turnover in the reservoir microvilli is far more dynamic. Whereas F-actin turns over in minutes to hours in stereocilia, brush border microvilli, and filopodia (Barzik et al., 2014; Rzadzinska, 2004; Tyska and Mooseker, 2002), F-actin lifetimes are only a few tens of seconds in the microvilli of cellularizing embryos. In terms of morphology, reservoir microvilli are also much more heterogeneous than either gut microvilli or filopodia (Crawley et al., 2014; Faix et al., 2009; Figard et al., 2013). In electron micrographs, reservoir microvilli in cellularizing embryos appear as a mixture of finger-like projections, ruffles, and ruffles with fingers extending from them (Figard et al., 2013). The same morphologies and heterogeneity are also seen in the reservoir microvilli of macrophage and mastocytoma cells (Erickson and Trinkaus, 1976; Knutton et al., 1975; Petty et al., 1981), suggesting that these architectures are typical for cell surface reservoirs.

We suggest that both the non-uniform morphologies of protrusions in reservoirs as well as their fast F-actin turnover are functions of the underlying F-actin ultra-structure. Specifically, F-actin in heterogeneously shaped reservoirs may be relatively more disorganized than the highly ordered bundles of F-actin in homogeneous brush border microvilli or filopodia. Consistent with this, mouse mutations in F-actin crosslinkers (e.g. Villin, Espin, and Fimbrin), as well as mutations in F-actin/membrane tethers (e.g. Myosins

1A and 6, and Ezrin) result in brush border microvilli that look more like reservoir microvilli in their mixed sizes and shapes (Crawley et al., 2014; Hegan et al., 2012; Tyska et al., 2005). As a trade-off, reduced F-actin order in reservoir protrusions may allow for faster F-actin dynamics (Medalia et al., 2007), rendering the reservoir scaffold more plastic and so better able to respond to membrane supply and demand. In fact, reservoir microvilli may lack specific mechanisms for creating uniformity and stability, as these mechanisms would be unnecessary or possibly even unfavorable for a transient, plastic membrane reservoir.

Whatever its ultrastructure, our data argue that the F-actin scaffold within reservoir microvilli is largely regulated by the membrane economy: Membrane supply from exocytosis promotes F-actin assembly and reservoir maintenance, while membrane demand from furrow ingression promotes F-actin disassembly and reservoir depletion. On the supply side, exocytosis may deliver F-actin regulators (Cao et al., 2008; Palamidessi et al., 2008). Alternatively, exocytosis could stimulate F-actin assembly by relieving plasma membrane tension, which normally antagonizes F-actin polymerization (Dai and Sheetz, 1995). Plasma membrane tension is a measure of the deformability of the membrane (Diz-Muñoz et al., 2013). Delivery of more membrane via exocytosis would make the membrane easier to deform (Gauthier et al., 2012; 2009), therefore reducing resistance to actin monomer addition at filament plus ends abutting the membrane (Diz-Muñoz et al., 2013; Keren et al., 2008; Mogilner and Oster, 1996; Mogilner and Rubinstein, 2005; Theriot and Mitchison, 1991). Thus, during cellularization, membrane supply via exocytosis may create a mechanically permissive environment for actin polymerization, which with the right complement of F-actin elongation factors (e.g. Ena; Grevengoed, 2003), supports the formation and maintenance of the reservoir.

On the demand side, furrow ingression controls disassembly of microvillar F-actin. One simple model is that membrane tension is also the signal that couples furrow ingression with F-actin disassembly. Given that membrane flows directly from the microvilli to the furrows (Figard et al., 2013; Lecuit and Wieschaus, 2000), we suggest that a pulling force likely occurs in the direction of furrow ingression. Furrow pulling could be communicated to the microvillar F-actin via plasma membrane tension, which as discussed above, can control F-actin dynamics. Plasma membrane tension is known to integrate spatially distant forces and F-actin dynamics over entire cell surfaces during other cell shape changes like spreading, crawling, and phagocytosis (Herant et al., 2005; Houk et al., 2012; Keren et al., 2008; Raucher and Sheetz, 2000). In those shape changes, high plasma membrane tension resists deformation and so antagonizes F-actin polymerization and protrusion. Very high tension can even buckle or crush F-actin (Mogilner and Rubinstein, 2005). In the case of cellularizing embryos, furrow pulling may generate enough plasma membrane tension so that the plasma membrane itself antagonizes the elongation of reservoir microvilli when exocytosis stops and membrane amount becomes limiting. Alternatively, plasma membrane tension could also elicit mechanosensitive signals that act through the cytoplasm to change the activity of F-actin capping or bundling proteins to link furrow ingression and microvillar F-actin disassembly (Diz-Muñoz et al., 2013; Goehring and Grill, 2013; Houk et al., 2012).

Finally, in regard to the relationship between membrane trafficking and reservoir usage, our data shows something distinct from what the cultured cell work predicts. For cell spreading

and particle engulfment in cultured cells, reservoir usage and exocytosis occur sequentially. That is, reservoirs unfold in an initial fast phase of cell surface expansion; and only after the reservoir is completely depleted does a spike in membrane tension trigger exocytosis of new membrane (Gauthier et al., 2011; Masters et al., 2013). In contrast, in cellularizing embryos, exocytosis provides membrane to the microvillar reservoir before as well as during unfolding. This is the first time that this sequence of membrane handling has been reported. What's more, our observations for cellularization suggest that regulated exocytosis purposefully puts membrane into cell surface reservoirs for anticipated events of cell surface expansion. This raises the possibility that reservoir formation is regulated with respect to events requiring cell surface expansion, like cytokinesis and embryonic morphogenesis. Moving forward, reservoir studies in cellularizing embryos will complement work in cultured cells because the modes of coordinating exocytosis and reservoir dynamics are distinct between these cell types and contexts. In addition, available secretory and exocytic mutants that impact furrow ingression during cellularization (e.g. Lava lamp, Sec5, Rab11, Syntaxin-1) present a singular opportunity to interrogate the molecular mechanisms linking exocytosis and reservoir dynamics.

Experimental Procedures

Fly stocks

Stocks for live imaging were: OreR, Sqh-GFP (Royou et al., 2004), Venus-PH-PLC5 (Figard et al., 2013), Utrophin-mCherry (this paper), Spider-GFP (Morin et al., 2001) and UASGalT-GFP (Snapp et al., 2004) crossed with mat67tub-GAL4.

Confocal imaging and analysis

All confocal imaging was done on a Zeiss LSM710 microscope. For fixed or live imaging, either a 63X oil-immersion objective (NA 1.4) or a 40X water-immersion objective (NA 1.2) was used, respectively. For live confocal imaging, embryos were mounted as described (Figard and Sokac, 2011).

For 4D imaging, Z-stacks spanning −5 μm of embryo surface were collected at 5 minute intervals using a pinhole = 1AU. Images were collapsed into maximum intensity Z-projections, and fluorescence quantified in ImageJ. Additional projection types (average intensity and summed stack) gave the same trends. Wild-type embryos (Figure 4B; Figure S2A–C) that required ≥75 minutes to complete cellularization were excluded due to concerns about phototoxicity (Figard et al., 2013). Normalization is detailed in the Supplemental Experimental Procedures.

For WGA crosslinking experiments, images were collected at the embryo cross-section. To quantify MV F-actin levels in WGA^{Ax488}-injected embryos, Utrophin-mCherry fluorescence was measured in a series of $5\mu m^2$ boxes drawn along the surface of the embryo. Furrow length per box was measured from the embryo surface to the furrow tip. Fluorescence intensities and furrow lengths were normalized as a fraction of the maximum value per embryo. Embryos were included for analysis if the ratio of shortest to longest furrow lengths were ≤0.5. We considered this ratio indicative of the "bowing" phenotype, and excluded 3

out of 11 embryos based on this criterion. To quantify Golgi levels in WGA^{Ax594}-injected embryos, GalT-GFP fluorescence was quantified in a series of $10\mu m^2$ boxes under the nuclei. To quantify secretory vesicle levels in WGA^{Ax594}-injected embryos, SpiderGFP fluorescence intensity was quantified from a series of $10\mu m^2$ boxes under the furrows. For both GalT-GFP and Spider-GFP, fluorescence intensities were normalized as a fraction of the minimum value.

For FRAP, experiments were done at the embryo's cross-section by bleaching a $3\mu m^2$ box at the apical surface using 100% laser power for 25 bleaching iterations, using the zoom bleach function. Images were then collected at 2-second intervals to track recovery. For FRAP analysis, fluorescence intensity in the bleached region (FRAP) and an adjacent, non-bleached region (REF) was quantified. Fluorescence at each time point was normalized as: $I_{NormA} = (I_{FRAP}*I_{REF\text{-}Pre\text{-}bleach})/(I_{FRAP\text{-}Pre\text{-}bleach}*I_{REF})$, where I_{FRAP} is the fluorescence in the bleached region at that time, $I_{REF\text{-}Pre\text{-}bleach}$ is the pre-bleach fluorescence in an unbleached region, $I_{FRAP\text{-}Pre\text{-}bleach}$ is the pre-bleach fluorescence in the FRAP region, and I_{REF} is the fluorescence in the unbleached region at that time point (Hardy, 2001). Recovery was fit to a single-exponential fit in MATLAB, and half time to recovery was calculated. Mobile fraction was calculated by the equation: Mobile fraction = $(I_{max}\text{-}I_{min})\text{-}(1\text{-}I_{min})$, in which I_{max} is the final recovered fluorescence value calculated in MATLAB, and I_{min} is the first post-bleaching fluorescence value.

TIRF imaging and analysis

Dechorionated embryos were sorted and staged in PBS, then sandwiched with a small drop of PBS between a coverslip (24×50 mm, #1.5 thickness, VWR) and a thin (1mm) slice of 1.5% agar (Skinner et al., 2013). Imaging was done on a Nikon Ti microscope equipped with a TIRF illuminator and a 100X TIRF objective, using a 561 nm laser. After manual adjustment of the TIRF angle, movies were captured at 1-second intervals for 3 minutes. The lifetimes of "head-on" microvilli were quantified by measuring fluorescence intensity over time, which increased and then decreased during protrusion and retraction, respectively. Minimum fluorescence values on either side of the peak were set as the "start" and "end" times of protrusion. The lifetimes of "lying-down" microvilli were quantified by measuring the length of the protrusion from base to tip throughout protrusion and retraction. Only movies with clear "start" and "end" points for a single protrusion were included in analysis.

Statistical analysis

Significance was determined by either Student's t-test or 1-way ANOVA with Holm-Sidak post-hoc test.

Supplementary Material

Refer to Web version on PubMed Central for supplementary material.

Acknowledgments

We thank BCM colleagues Zenghui Xue, Dr. Heng Xu, and Dr. Leonardo Sepúlveda for assistance with FRAP imaging and data analysis. We thank Dr. Herbert Levine (Rice University) and Dr. Alex Mogilner (New York University) for discussing results; and Dr. Adam Martin (MIT) for critiquing the manuscript. For the majority of

this work, L.F. was enrolled in the Integrative Molecular and Biomedical Sciences Program at BCM, which is partially supported by NIH grant T32 GM008231. Work in the Sokac lab was supported by NIH grant R01 GM115111. Work in the Golding lab was supported by NIH grant R01 GM082837; NSF grants PHY 1147498, PHY-1430124, and PHY-1427654; a John S. Dunn Foundation Collaborative Research Award; and Welch Foundation grant Q-1759. We also thank the Computational and Integrative Biomedical Research Center at BCM for providing computing resources.

References

Acharya S, Laupsien P, Wenzl C, Yan S, Groβhans J. Function and dynamics of *slam* in furrow formation in early *Drosophila* embryo. Dev. Biol. 2014; 386:371–384. [PubMed: 24368071]

Babu P, Bryan JD, Panek HR, Jordan SL, Forbrich BM, Kelley SC, Colvin RT, Robinson LC. Plasma membrane localization of the Yck2p yeast casein kinase 1 isoform requires the C-terminal extension and secretory pathway function. J. Cell. Sci. 2002; 115:4957–4968. [PubMed: 12432082]

Barzik M, McClain LM, Gupton SL, Gertler FB. Ena/VASP regulates mDia2-initiated filopodial length, dynamics, and function. Mol. Biol. Cell. 2014; 25:2604–2619. [PubMed: 24989797]

Breitsprecher D, Koestler SA, Chizhov I, Nemethova M, Mueller J, Goode BL, Small JV, Rottner K, Faix J. Cofilin cooperates with fascin to disassemble filopodial actin filaments. J.Cell. Sci. 2011; 124:3305–3318. [PubMed: 21940796]

Burgess RW, Deitcher DL, Schwarz TL. The synaptic protein syntaxin1 is required for cellularization of *Drosophila* embryos. J. Cell. Biol. 1997; 138:861–875. [PubMed: 9265652]

Burkel BM, von Dassow G, Bement WM. Versatile fluorescent probes for actin filaments based on the actin-binding domain of utrophin. Cell. Motil. Cytoskeleton. 2007; 64:822–832. [PubMed: 17685442]

Cao J, Albertson R, Riggs B, Field CM, Sullivan W. Nuf, a Rab11 effector, maintains cytokinetic furrow integrity by promoting local actin polymerization. J. Cell. Biol. 2008; 182:301–313. [PubMed: 18644888]

Charras GT, Yarrow JC, Horton MA, Mahadevan L, Mitchison TJ. Non equilibration of hydrostatic pressure in blebbing cells. Nature. 2005; 435:365–369. [PubMed: 15902261]

Cheng JPX, Mendoza-Topaz C, Howard G, Chadwick J, Shvets E, Cowburn AS, Dunmore BJ, Crosby A, Morrell NW, Nichols BJ. Caveolae protect endothelial cells from membrane rupture during increased cardiac output. J. Cell. Biol. 2015; 211:53–61. [PubMed: 26459598]

Clark AG, Wartlick O, Salbreux G, Paluch EK. Stresses at the cell surface during animal cell morphogenesis. Curr. Biol. 2014; 24:R484–R494. [PubMed: 24845681]

Coué M, Brenner SL, Spector I, Korn ED. Inhibition of actin polymerization by latrunculin A. FEBS Lett. 1987; 213:316–318. [PubMed: 3556584]

Crawley SW, Mooseker MS, Tyska MJ. Shaping the intestinal brush border. J. Cell. Biol. 2014; 207:441–451. [PubMed: 25422372]

Dai J, Sheetz MP. Regulation of endocytosis, exocytosis, and shape by membrane tension. Cold Spring Harb. Symp. Quant. Biol. 1995; 60:567–571. [PubMed: 8824429]

Davis LI, Blobel G. Identification and characterization of a nuclear pore complex protein. Cell. 1986; 45:699–709. [PubMed: 3518946]

Diz-Muñoz A, Fletcher DA, Weiner OD. Use the force: membrane tension as an organizer of cell shape and motility. Trends Cell. Biol. 2013; 23:47–53. [PubMed: 23122885]

Erickson CA, Trinkaus JP. Microvilli and blebs as sources of reserve surface membrane during cell spreading. Exp. Cell. Res. 1976; 99:375–384. [PubMed: 1269533]

Fabrowski P, Necakov AS, Mumbauer S, Loeser E, Reversi A, Streichan S, Briggs JAG, De Renzis S. Tubular endocytosis drives remodelling of the apical surface during epithelial morphogenesis in *Drosophila* . Nat. Commun. 2013; 4:2244. [PubMed: 23921440]

Faix J, Breitsprecher D, Stradal TEB, Rottner K. Filopodia: Complex models for simple rods. Int. J. Biochem. Cell Biol. 2009; 41:1656–1664. [PubMed: 19433307]

Figard L, Sokac AM. A membrane reservoir at the cell surface: unfolding the plasma membrane to fuel cell shape change. Bioarchitecture. 2014; 4:39–46. [PubMed: 24844289]

Figard L, Sokac AM. Imaging cell shape change in living *Drosophila* embryos. J. Vis. Exp. 2011; 49:e2503.

Figard L, Xu H, Garcia HG, Golding I, Sokac AM. The plasma membrane flattens out to fuel cell-surface growth during *Drosophila* cellularization. Dev. Cell. 2013; 27:648–655. [PubMed: 24316147]

Frescas D, Mavrakis M, Lorenz H, Delotto R, Lippincott-Schwartz J. The secretory membrane system in the *Drosophila* syncytial blastoderm embryo exists as functionally compartmentalized units around individual nuclei. J. Cell. Biol. 2006; 173:219–230. [PubMed: 16636144]

Fullilove SL, Jacobson AG. Nuclear elongation and cytokinesis in *Drosophila montana* . Dev. Biol. 1971; 26:560–577. [PubMed: 5167431]

Gauthier NC, Fardin MA, Roca-Cusachs P, Sheetz MP. Temporary increase in plasma membrane tension coordinates the activation of exocytosis and contraction during cell spreading. Proc. Natl. Acad. Sci. USA. 2011; 108:14467–14472. [PubMed: 21808040]

Gauthier NC, Masters TA, Sheetz MP. Mechanical feedback between membrane tension and dynamics. Trends Cell Biol. 2012; 22:527–535. [PubMed: 22921414]

Gauthier NC, Rossier OM, Mathur A, Hone JC, Sheetz MP. Plasma membrane area increases with spread area by exocytosis of a GPI-anchored protein compartment. Mol. Biol. Cell. 2009; 20:3261–3272. [PubMed: 19458190]

Goehring NW, Grill SW. Cell polarity: mechanochemical patterning. Trends Cell. Biol. 2013; 23:72–80. [PubMed: 23182746]

Grevengoed EE, Fox DT, Gates J, Peifer M. Balancing different types of actin polymerization at distinct sites: roles for Abelson kinase and Enabled. J. Cell. Biol. 2003; 163:1267–1279. [PubMed: 14676307]

Groulx N, Boudreault F, Orlov SN, Grygorczyk R. Membrane reserves and hypotonic cell swelling. J. Membrane Biol. 2006; 214:43–56. [PubMed: 17598067]

Hardy LR. Fluorescence Recovery After Photobleaching (FRAP) with a focus on F-actin. Curr. Protoc. Neurosci. 2012:12.17.1–12.17.12. [PubMed: 23093351]

Hegan PS, Giral H, Levi M, Mooseker MS. Myosin VI is required for maintenance of brush border structure, composition, and membrane trafficking functions in the intestinal epithelial cell. Cytoskeleton. 2012; 69:235–251. [PubMed: 22328452]

Heinrich D, Ecke M, Jasnin M, Engel U, Gerisch G. Reversible membrane pearling in live cells upon destruction of the actin cortex. Biophys. J. 2014; 106:1079–1091. [PubMed: 24606932]

Herant M, Heinrich V, Dembo M. Mechanics of neutrophil phagocytosis: behavior of the cortical tension. J. Cell. Sci. 2005; 118:1789–1797. [PubMed: 15827090]

Holt GD, Snow CM, Senior A, Haltiwanger RS, Gerace L, Hart GW. Nuclear pore complex glycoproteins contain cytoplasmically disposed O-linked N acetylglucosamine. J. Cell. Biol. 1987; 104:1157–1164. [PubMed: 3571327]

Houk AR, Jilkine A, Mejean CO, Boltyanskiy R, Dufresne ER, Angenent SB, Altschuler SJ, Wu LF, Weiner OD. Membrane tension maintains cell polarity by confining signals to the leading edge during neutrophil migration. Cell. 2012; 148:175–188. [PubMed: 22265410]

Kapustina M, Elston TC, Jacobson K. Compression and dilation of the membrane-cortex layer generates rapid changes in cell shape. J. Cell. Biol. 2013; 200:95–108. [PubMed: 23295349]

Keren K, Pincus Z, Allen GM, Barnhart EL, Marriott G, Mogilner A, Theriot JA. Mechanism of shape determination in motile cells. Nature. 2008; 453:475–480. [PubMed: 18497816]

Knutton S, Sumner MC, Pasternak CA. Role of microvilli in surface changes of synchronized P815Y mastocytoma cells. J. Cell. Biol. 1975; 66:568–576. [PubMed: 1158972]

Lecuit T, Samanta R, Wieschaus E. *slam* encodes a developmental regulator of polarized membrane growth during cleavage of the *Drosophila* embryo. Dev. Cell. 2002; 2:425–436. [PubMed: 11970893]

Lecuit T, Wieschaus E. Polarized insertion of new membrane from a cytoplasmic reservoir during cleavage of the *Drosophila* embryo. J. Cell. Biol. 2000; 150:849–860. [PubMed: 10953008]

Lee DM, Harris TJ. Coordinating the cytoskeleton and endocytosis for regulated plasma membrane growth in the early *Drosophila* embryo. Bioarchitecture. 2014; 4:68–74. [PubMed: 24874871]

Martin AC, Gelbart M, Fernandez-Gonzalez R, Kaschube M, Wieschaus EF. Integration of contractile forces during tissue invagination. J. Cell. Biol. 2010; 188:735–749. [PubMed: 20194639]

Masters TA, Pontes B, Viasnoff V, Li Y, Gauthier NC. Plasma membrane tension orchestrates membrane trafficking, cytoskeletal remodeling, and biochemical signaling during phagocytosis. Proc. Natl. Acad. Sci. USA. 2013; 110:11875–11880. [PubMed: 23821745]

Mavor LM, Miao H, Zuo Z, Holly RM, Xie Y, Loerke D, Blankenship JT. Rab8 directs furrow ingression and membrane addition during epithelial formation in *Drosophila* melanogaster. Development. 2016; 143:892–903. [PubMed: 26839362]

Medalia O, Beck M, Ecke M, Weber I, Neujahr R, Baumeister W, Gerisch G. Organization of Actin Networks in Intact Filopodia. Curr. Biol. 2007; 17:79–84. [PubMed: 17208190]

Mogilner A, Oster G. Cell motility driven by actin polymerization. Biophys. J. 1996; 71:3030–3045. [PubMed: 8968574]

Mogilner A, Rubinstein B. The Physics of Filopodial Protrusion. Biophys. J. 2005; 89:782–795. [PubMed: 15879474]

Mooseker MS, Tilney LG. Organization of an actin filament-membrane complex. Filament polarity and membrane attachment in the microvilli of intestinal epithelial cells. J. Cell. Biol. 1975; 67:725–743. [PubMed: 1202021]

Morin X, Daneman R, Zavortink M, Chia W. A protein trap strategy to detect GFP-tagged proteins expressed from their endogenous loci in *Drosophila* . Proc. Natl. Acad. Sci. USA. 2001; 98:15050–15055. [PubMed: 11742088]

Murthy M, Teodoro RO, Miller TP, Schwarz TL. Sec5, a member of the exocyst complex, mediates *Drosophila* embryo cellularization. Development. 2010; 137:2773–2783. [PubMed: 20630948]

Nowotarski SH, McKeon N, Moser RJ, Peifer M. The actin regulators Enabled and Diaphanous direct distinct protrusive behaviors in different tissues during *Drosophila* development. Mol. Biol. Cell. 2014; 25:3147–3165. [PubMed: 25143400]

Palamidessi A, Frittoli E, Garré M, Faretta M, Mione M, Testa I, Diaspro A, Lanzetti L, Scita G, Di Fiore PP. Endocytic trafficking of Rac is required for the spatial restriction of signaling in cell migration. Cell. 2008; 134:135–147. [PubMed: 18614017]

Papoulas O, Hays TS, Sisson JC. The golgin Lava lamp mediates dynein based Golgi movements during *Drosophila* cellularization. Nat. Cell. Biol. 2004; 7:612–618. [PubMed: 15908943]

Petty HR, Hafeman DG, McConnell HM. Disappearance of macrophage surface folds after antibody-dependent phagocytosis. J. Cell. Biol. 1981; 89:223–229. [PubMed: 7251651]

Pollard TD, Borisy GG. Cellular motility driven by assembly and disassembly of actin filaments. Cell. 2003; 112:453–465. [PubMed: 12600310]

Raucher D, Sheetz MP. Cell spreading and lamellipodial extension rate is regulated by membrane tension. J. Cell. Biol. 2000; 148:127–136. [PubMed: 10629223]

Royou A, Field C, Sisson JC, Sullivan W, Karess R. Reassessing the role and dynamics of nonmuscle myosin II during furrow formation in early *Drosophila* embryos. Mol. Biol. Cell. 2004; 15:838–850. [PubMed: 14657248]

Rzadzinska AK, Schneider ME, Davies C, Riordan GP, Kachar B. An actin molecular treadmill and myosins maintain stereocilia functional architecture and self-renewal. J. Cell. Biol. 2004; 164:887–897. [PubMed: 15024034]

Sciaky N, Presley J, Smith C, Zaal KJ, Cole N, Moreira JE, Terasaki M, Siggia E, Lippincott-Schwartz J. Golgi tubule traffic and the effects of brefeldin A visualized in living cells. J. Cell. Biol. 1997; 139:1137–1155. [PubMed: 9382862]

Sedzinski J, Biro M, Oswald A, Tinevez JY, Salbreux G, Paluch E. Polar actomyosin contractility destabilizes the position of the cytokinetic furrow. Nature. 2011; 476:462–466. [PubMed: 21822289]

Sinha B, Köster D, Ruez R, Gonnord P, Bastiani M, Abankwa D, Stan RV, Butler-Browne G, Vedie B, Johannes L, Morone N, Parton RG, Raposo G, Sens P, Lamaze C, Nassoy P. Cells respond to mechanical stress by rapid disassembly of caveolae. Cell. 2011; 144:402–413. [PubMed: 21295700]

Sisson JC, Field C, Ventura R, Royou A, Sullivan W. Lava lamp, a novel peripheral golgi protein, is required for *Drosophila melanogaster* cellularization. J. Cell. Biol. 2000; 151:905–918. [PubMed: 11076973]

Skinner SO, Sepúlveda LA, Xu H, Golding I. Measuring mRNA copy number in individual *Escherichia coli* cells using single-molecule fluorescent *in situ* hybridization. Nat. Protoc. 2013; 8:1100–1113. [PubMed: 23680982]

Snapp EL, Iida T, Frescas D, Lippincott-Schwartz J, Lilly MA. The fusome mediates intercellular endoplasmic reticulum connectivity in *Drosophila* ovarian cysts. Mol. Biol. Cell. 2004; 15:4512–4521. [PubMed: 15292454]

Stein JA, Broihier HT, Moore LA, Lehmann R. Slow as molasses is required for polarized membrane growth and germ cell migration in *Drosophila* . Development. 2002; 129:3925–3934. [PubMed: 12135929]

Sweeton D, Parks S, Costa M, Wieschaus E. Gastrulation in *Drosophila*: the formation of the ventral furrow and posterior midgut invaginations. Development. 1991; 112:775–789. [PubMed: 1935689]

Tan PY, Zaidel-Bar R. Transient membrane localization of SPV-1 drives cyclical actomyosin contractions in the *C. elegans* spermatheca. Curr. Biol. 2015; 25:141–151. [PubMed: 25532891]

Theriot JA, Mitchison TJ. Actin microfilament dynamics in locomoting cells. Nature. 1991; 352:126–131. [PubMed: 2067574]

Tyska MJ, Mackey AT, Huang J-D, Copeland NG, Jenkins NA, Mooseker MS. Myosin-1a is critical for normal brush border structure and composition. Mol. Biol. Cell. 2005; 16:2443–2457. [PubMed: 15758024]

Tyska MJ, Mooseker MS. MYO1A (brush border myosin I) dynamics in the brush border of LLC-PK1-CL4 cells. Biophys. J. 2002; 82:1869–1883. [PubMed: 11916846]

Wenzl C, Yan S, Laupsien P, Groβhans J. Localization of RhoGEF2 during *Drosophila* cellularization is developmentally controlled by Slam. Mech. Dev. 2010; 127:371–384. [PubMed: 20060902]

Highlights

- Exocytosis adds membrane to a surface reservoir that unfolds to fuel furrow ingression
- F-actin deforms the reservoir into dynamic microvilli that are lost as furrows ingress
- Exocytosis (membrane supply) promotes microvillar F-actin assembly
- Furrow ingression (membrane demand) promotes microvillar F-actin disassembly

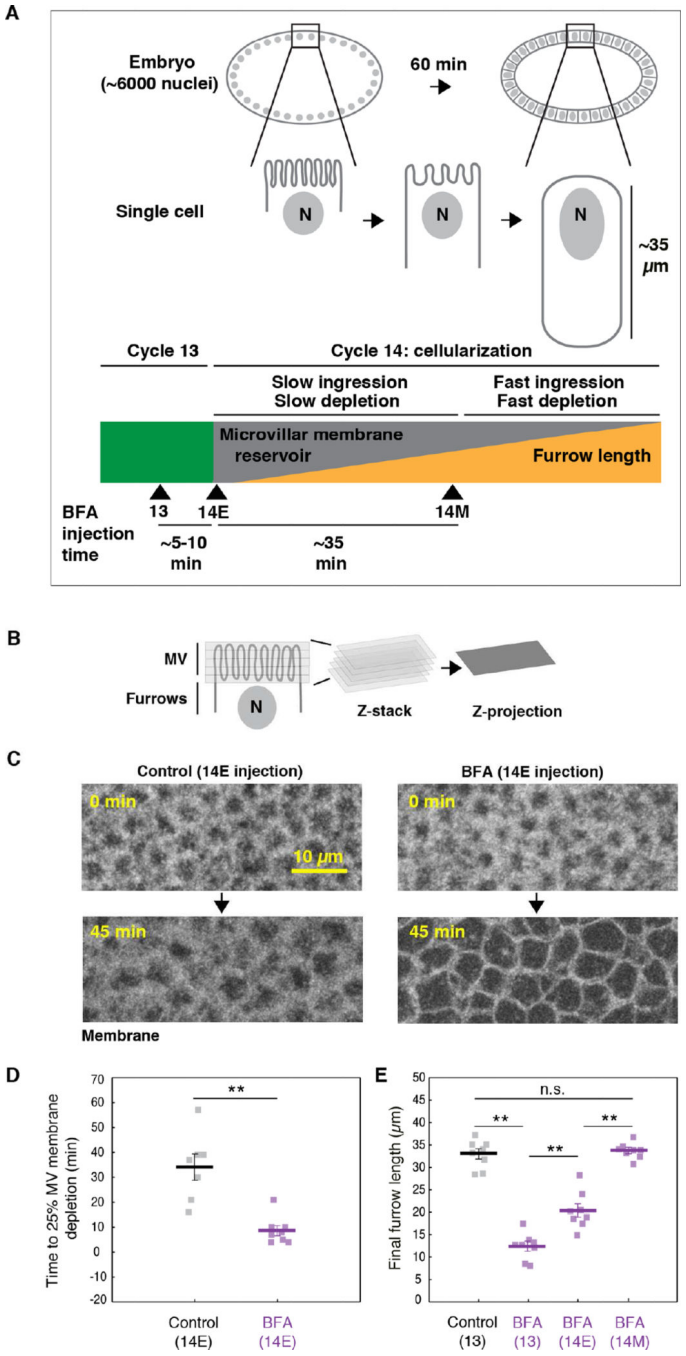

Figure 1. Exocytosis delivers membrane that is stored in a microvillar reservoir

(A) The progression of cellularization. Nuclei are labeled “N”. Green block indicates cycle 13. Gray/orange block indicates cellularization at cycle 14. Throughout cellularization, reservoir unfolding and depletion fuel furrow ingression. Arrowheads mark time of BFA injection in cycle 13 (13), early cellularization (14E), and mid-cellularization (14M).

(B) Time-lapse Z-stacks, encompassing the microvilli (MV), are collapsed into maximum intensity projections (Z-projections).

(C) Z-projections of Venus-PH-PLCδ in DMSO- (Control) or BFA-injected embryos show depletion of MV membrane over time. 0 minutes is onset of cellularization. Injection time 14E.

(D) Time to reach 25% depletion of MV membrane fluorescence for DMSO- (Control) or BFA-injected Venus-PH-PLCδ embryos. Injection time 14E. Each square represents one embryo (N≥7 embryos per condition; horizontal bold lines are mean ± SE; **p<0.001, Student's t-test).

(E) Final furrow lengths for DMSO- (Control) or BFA-injected Sqh-GFP embryos. Injection times indicated. Each square represents one embryo (N=8 embryos per condition; horizontal bold lines are mean ± SE; p<0.001, 1-way ANOVA; **p<0.001; n.s. indicates not significant; Holm-Sidak post-hoc test).

See also Figure S1.

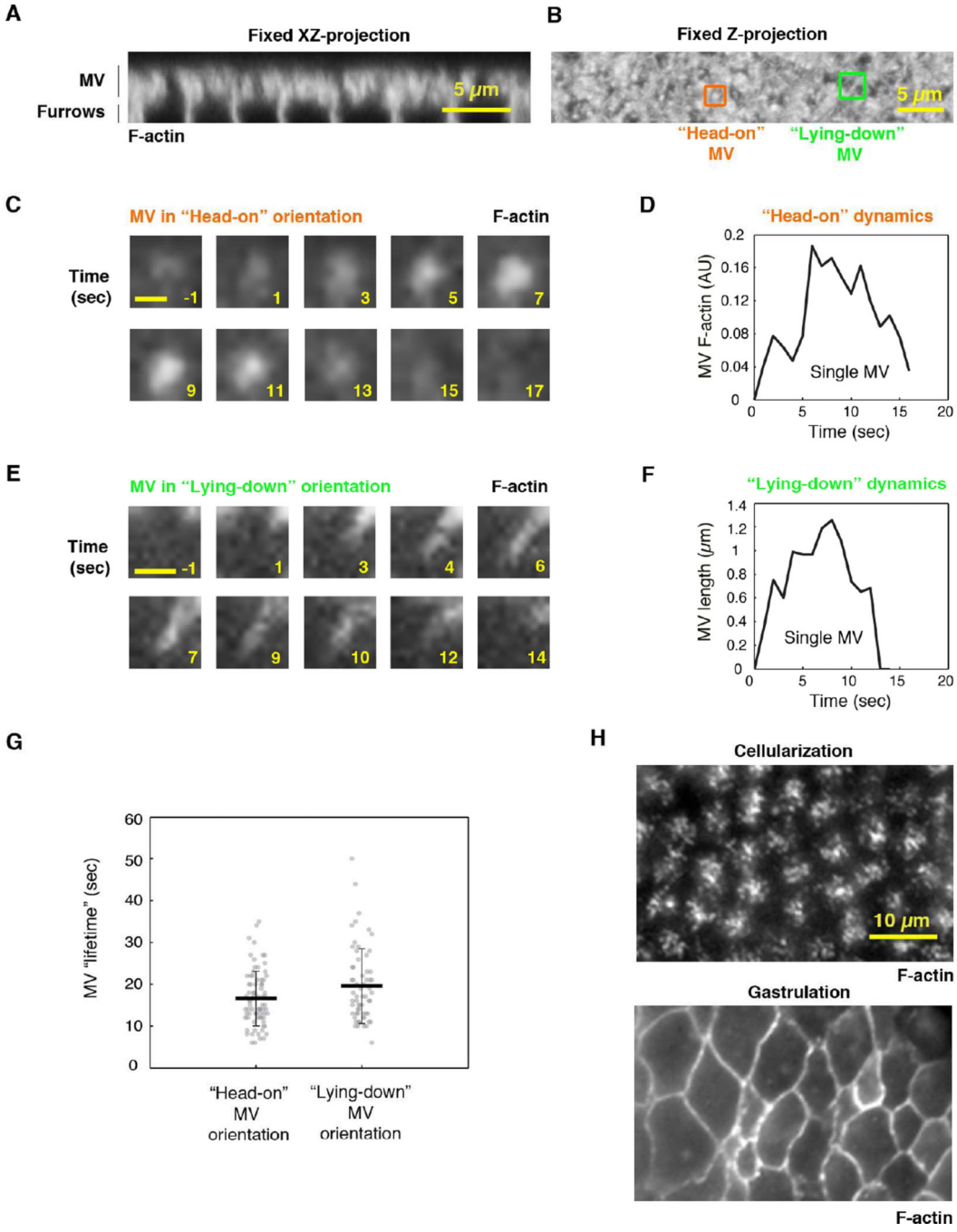

Figure 2. The microvillar F-actin scaffold is dynamic

(A) XZ projection of F-actin (Phalloidin^{Ax546}) in microvilli (MV) of a fixed wild-type embryo.

(B) Z-projection of embryo in (A). Example MV in two orientations: "head-on" MV (orange) grow orthogonal to the surface, and "lying-down" MV (green) grow parallel to the surface.

(C) Time-lapse TIRF images of an extending/retracting microvillus (F-actin; Utrophin-mCherry) in a “head-on” orientation. Numbers are seconds; 0 seconds marks onset of extension. Scale bar 0.5μm.

(D) F-actin fluorescence versus time for the microvillus in (C).

(E) Time-lapse TIRF images of an extending/retracting microvillus (F-actin; Utrophin-mCherry) in a “lying-down” orientation. Numbers are seconds; 0 seconds marks onset of extension. Scale bar 1 μm.

(F) Length versus time for the microvillus in (E).

(G) Lifetimes of MV in “head-on” and “lying-down” orientations. Each circle represents one microvillus (N>62 MV from 5 embryos per method; horizontal bold lines are mean ± SD).

(H) TIRF images of F-actin at the surface of Utrophin-mCherry embryos at cellularization or gastrulation. **See also** Movie S1.

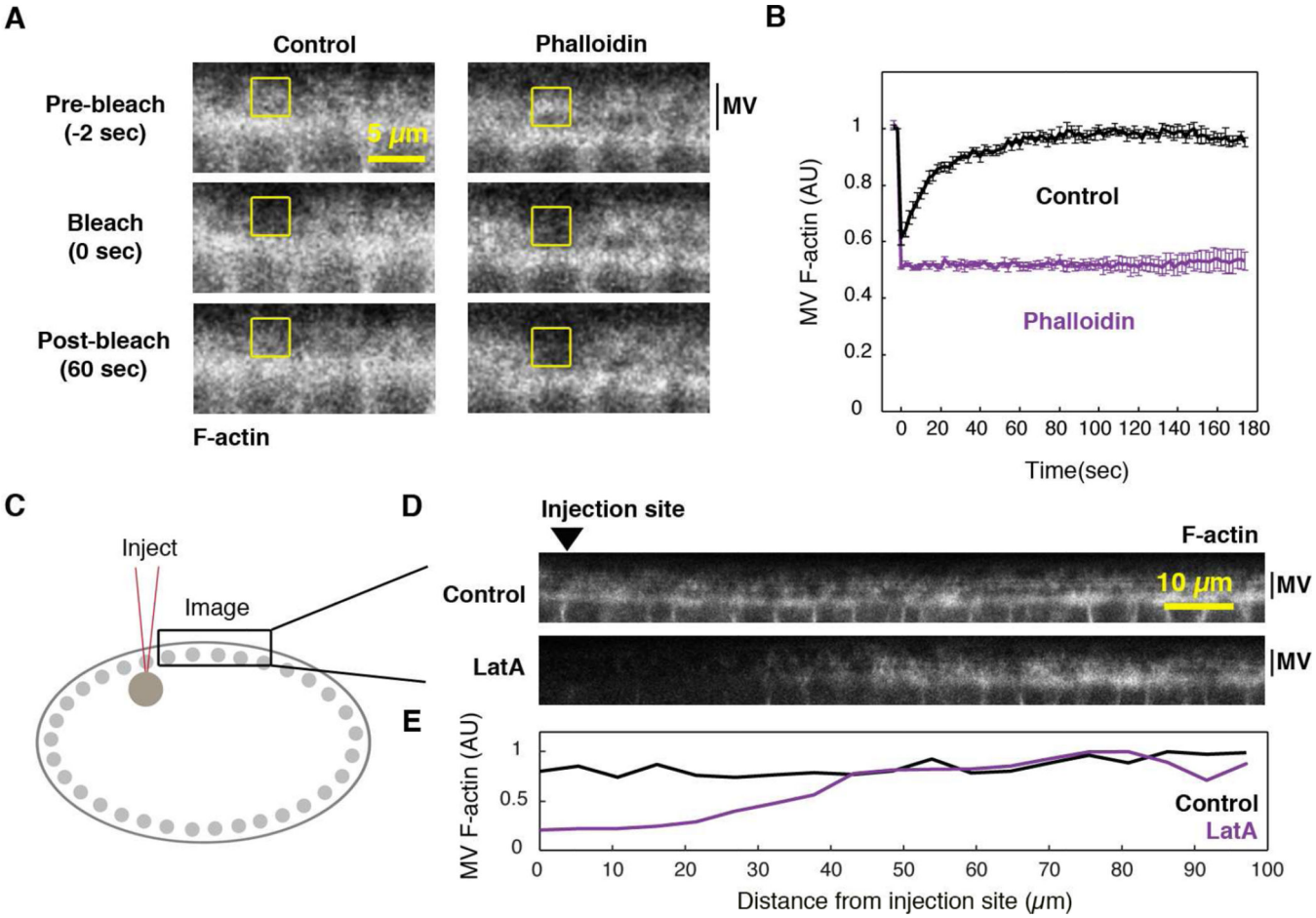

Figure 3. Dynamic F-actin is required to maintain the microvilli

(A) Time-lapse confocal cross-sections show FRAP of microvillar F-actin (MV; rhodamine G-actin) in buffer- (Control) or Phalloidin-injected embryos. Yellow box is the bleached region.

(B) MV F-actin FRAP in buffer- (Control) or Phalloidin-injected embryos (N≥4 embryos per condition; mean ± SE). 0 seconds is the first frame after bleaching.

(C) Representation of injection and imaging sites for (D).

(D) Confocal cross-sections of Utrophin-mCherry show F-actin levels ~1 min after injection of DMSO (Control) or LatA. Arrowhead marks injection site.

(E) MV F-actin fluorescence versus distance from injection site for embryos in (D).

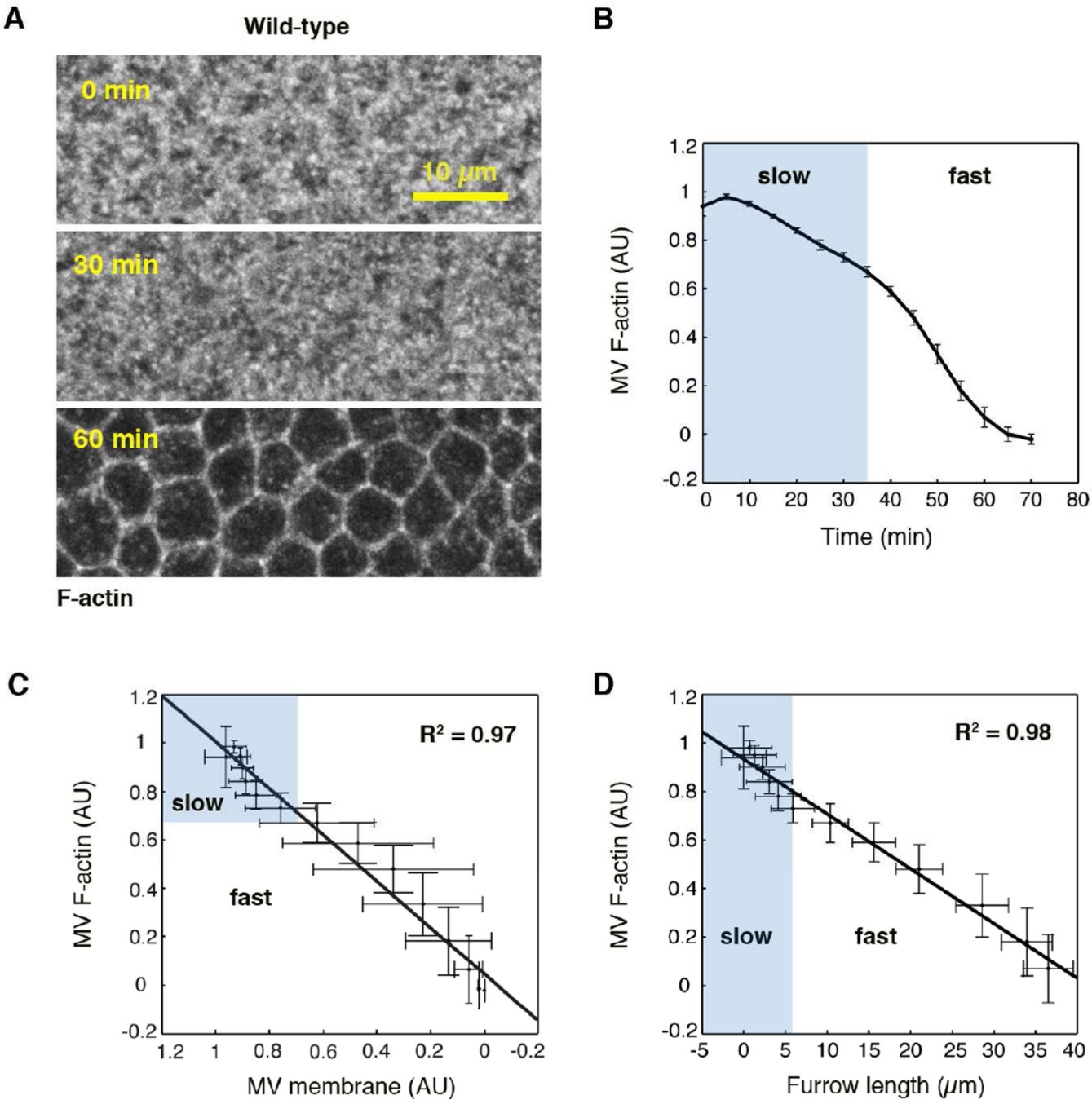

Figure 4. Microvillar F-actin is depleted *in sync* with furrow ingression

(A) Z-projections of Utrophin-mCherry show depletion of microvillar (MV) F-actin over time.

(B) MV F-actin fluorescence versus time during cellularization (N=12 embryos; mean ± SE).

(C) Average normalized MV F-actin fluorescence (N=12 embryos; mean ± SD) versus average normalized MV membrane fluorescence (Venus-PH-PLCδ; N=4 embryos; mean ± SD).

(D) Average normalized MV F-actin fluorescence versus furrow length (N=12 embryos; mean ± SD). For (B)–(D), slow ingression/depletion phase shaded in blue. Shading is based on transition from slow to fast phase as defined in Figard et al., 2013. For (C) and (D), line is a linear least-square fit.

See also Figure S2.

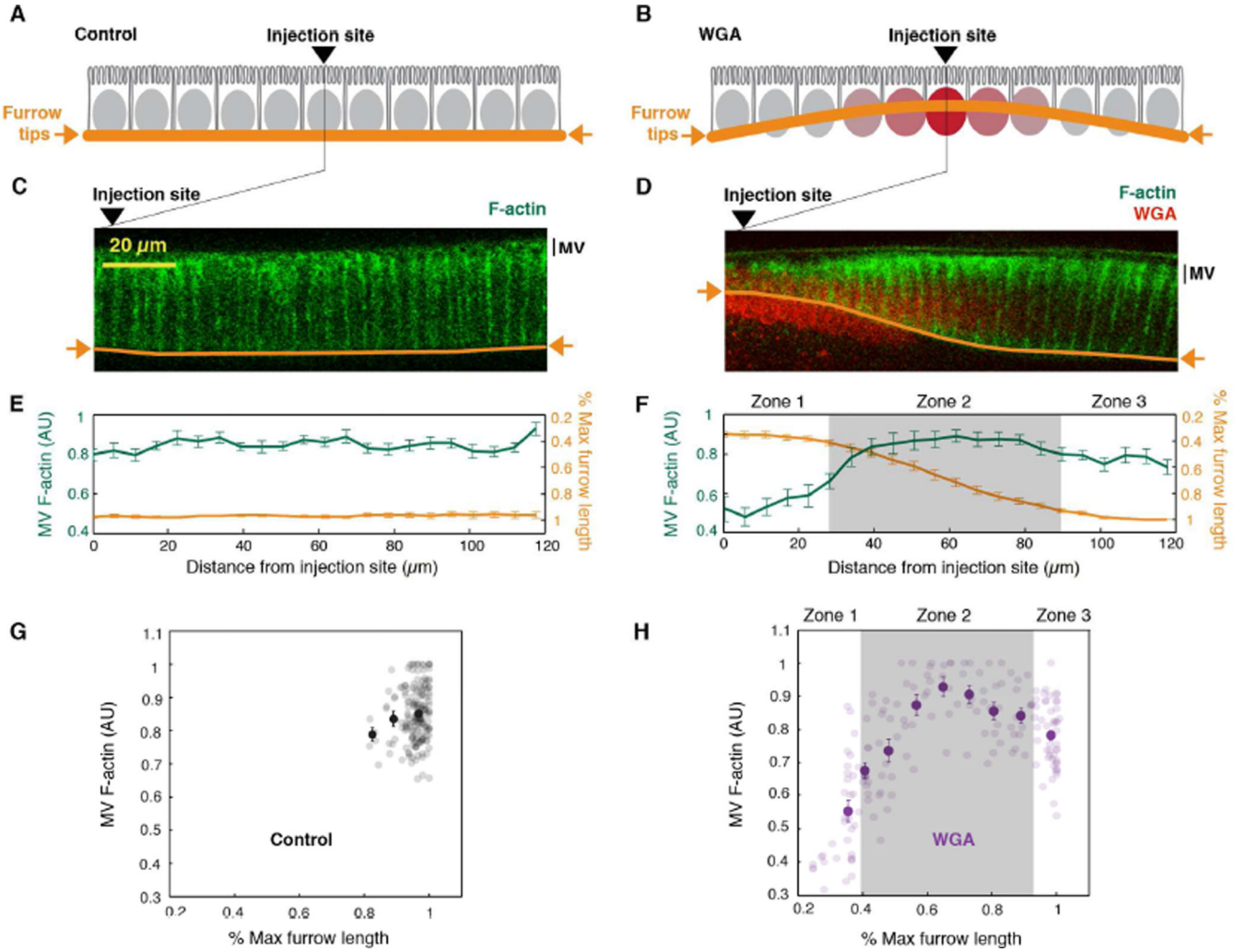

Figure 5. Microvillar F-actin depletion is coupled to furrow ingression

(A, B) The WGA nuclear crosslinking experiment. In (A) control embryos, furrow tips ingress between nuclei (gray ovals) making an even furrow front (orange line). In (B) WGA-injected embryos, crosslinked nuclei (red ovals) make a local barrier, impeding furrow ingression and generating a curved furrow front.

(C, D) Confocal cross-sections of microvillar F-actin (Utrophin-mCherry; green) in cellularizing embryos ~40 minutes after (C) buffer- (Control) or (D) WGA^{Ax488} injection (red). Channels are pseudocolored for presentation. Furrow tips traced (orange). Arrowheads mark injection sites.

(E, F) MV F-actin fluorescence (green) and furrow length (orange) versus distance from injection site in (E) buffer- (Control) or (F) WGA^{Ax488}-injected Utrophin-mCherry embryos (N=8 embryos per condition; mean ± SE).

(G, H) MV F-actin fluorescence versus percent max furrow length in (G) buffer- (Control) or (H) WGA^{Ax488}-injected Utrophin-mCherry embryos (N=176 data points from 8 embryos per condition). Dark circles represent binned data (mean ± SE). For (F and H), zones are as described in the Results.

See also Figure S3.

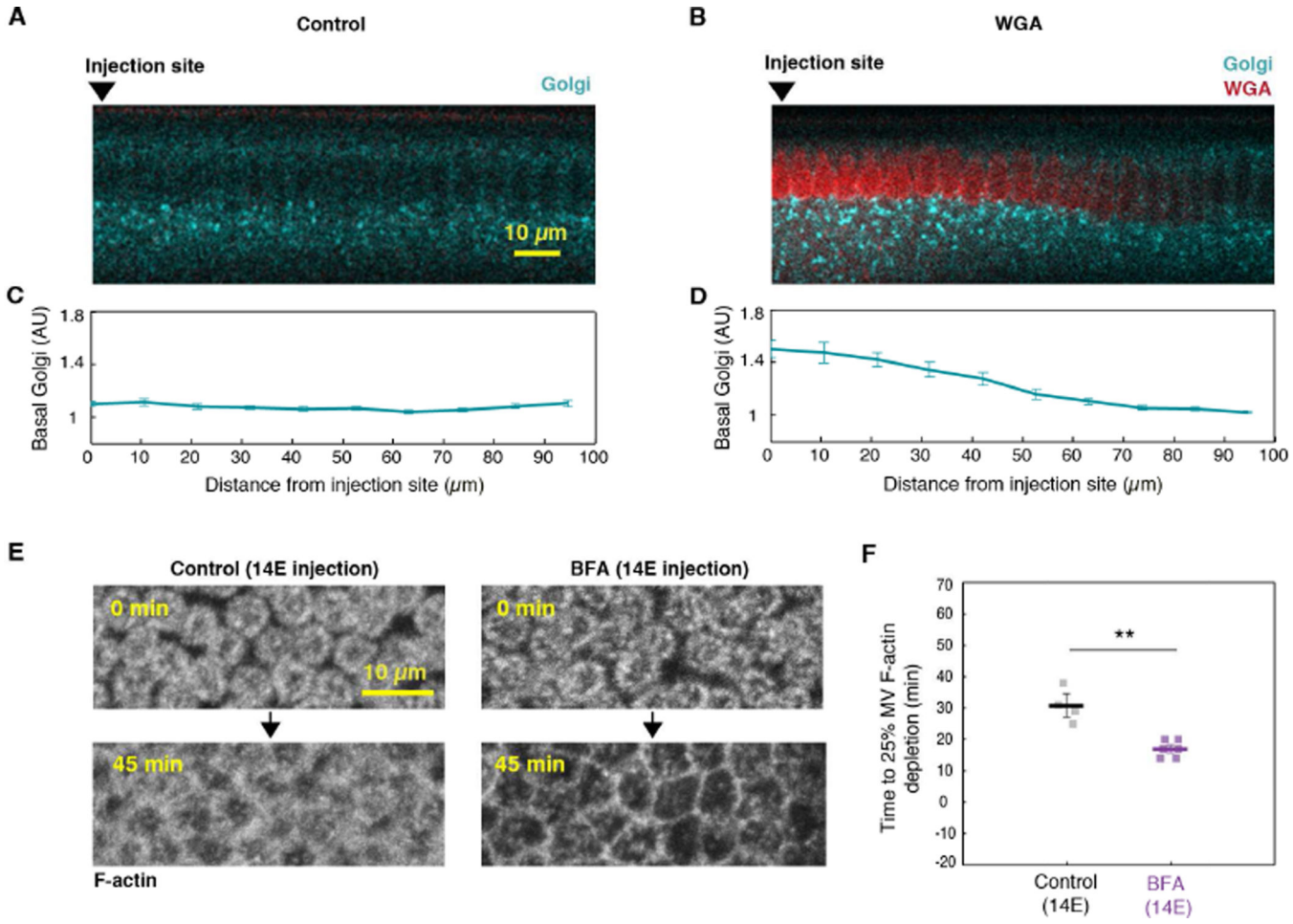

Figure 6. Exocytosis promotes microvillar F-actin assembly

(A, B) Confocal cross-sections of GalT-GFP (blue) in (A) buffer- (Control) and (B) WGA^{Ax594}-injected (red) embryos show Golgi bodies. Arrowheads mark injection sites. GalT-GFP channel is pseudocolored for presentation.

(C, D) Golgi fluorescence versus distance from the injection site in (C) buffer- (Control) and (D) WGA^{Ax594}-injected (red) GalT-GFP embryos (N=8 embryos per condition; mean ± SE).

(E) Z-projections of Utrophin-mCherry in DMSO- (Control) or BFA-injected embryos showing depletion of microvillar F-actin over time. 0 minutes is onset of cellularization.

(F) Time to reach 25% depletion of microvillar F-actin fluorescence in DMSO- (Control) or BFA-injected Utrophin-mCherry embryos. For (E) and (F), injection time 14E. Each square represents one embryo (N≥4 embryos per condition; horizontal bold lines are mean ± SE; **p<0.001, Student's t-test).

See also Figures S4 and S5.

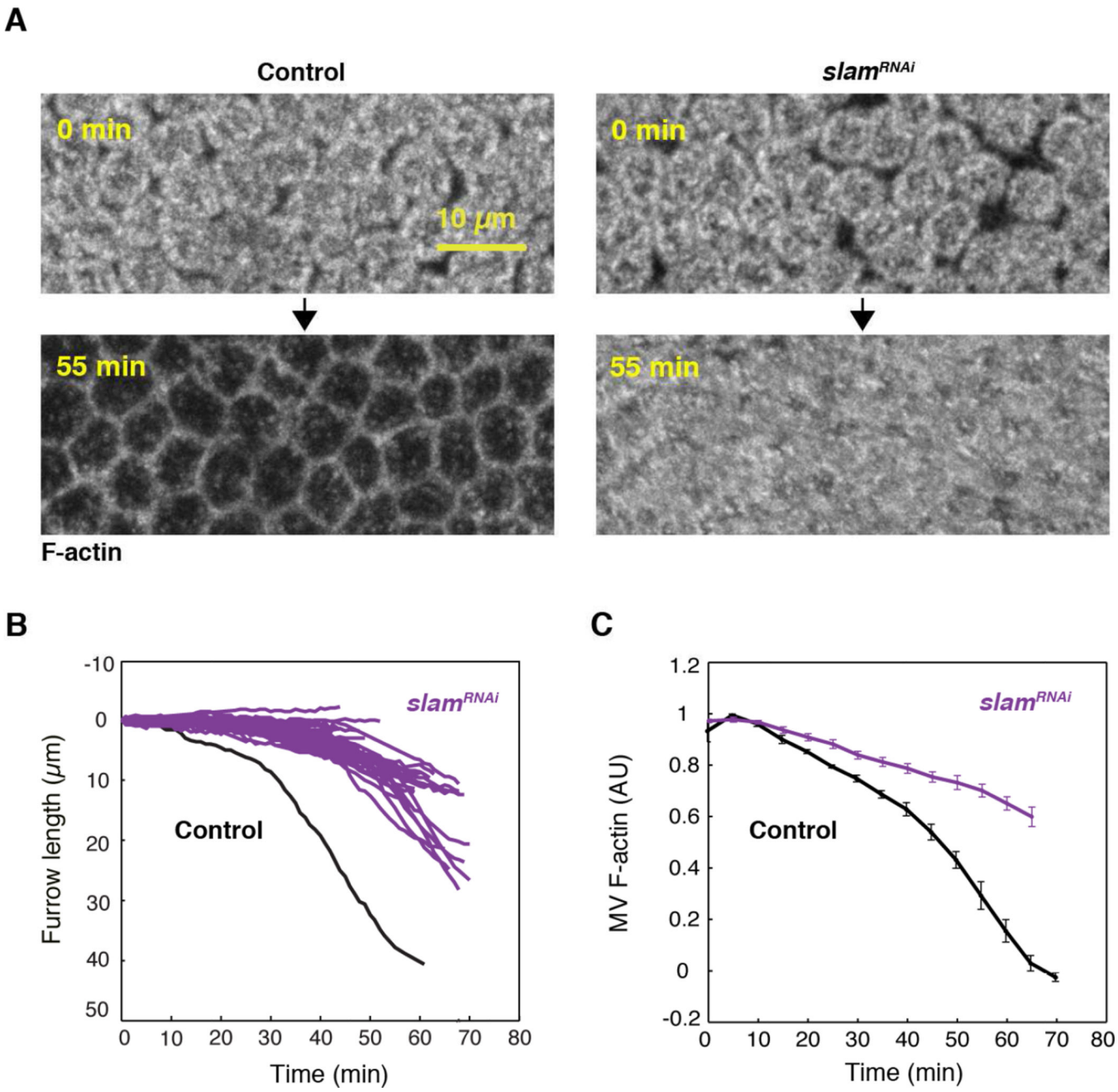

Figure 7. Furrow ingression regulates microvillar F-actin depletion

(A) Z-projections of Utrophin-mCherry in buffer-injected (Control) or *slam*^{RNAi} embryos showing microvillar F-actin over time.

(B) Furrow length versus time for Sqh-GFP embryos after *slam*^{RNAi} (purple; N=47 trajectories from 8 embryos). A typical furrow trajectory from a buffer-injected (Control) Sqh-GFP embryo is shown for comparison (black).

(C) Microvillar F-actin fluorescence versus time for Utrophin-mCherry embryos after *slam*^{RNAi} (purple) or buffer-injection (Control; black; N=12 or 6 embryos for *slam*^{RNAi} or controls, respectively; mean ± SE).